JASA Express Letters

APRIL 09 2025

Estimating sound pressure levels from distributed acoustic sensing data using 20 Hz fin whale calls

Léa Bouffaut ; Quentin Goestchel ; Robin André Rørstadbotnen ; Anthony Sladen ; Arthur Hartog; Holger Klinck

JASA Express Lett. 5, 040802 (2025)
https://doi.org/10.1121/10.0036351

JASA EXPRESS LETTERS ARTICLE asa.scitation.org/journal/jel

Estimating sound pressure levels from distributed acoustic sensing data using 20 Hz fin whale calls

Léa Bouffaut,[1,a] Quentin Goestchel,[2] Robin André Rørstadbotnen,[3] Anthony Sladen,[4] Arthur Hartog,[5] and Holger Klinck[1]

[1]K. Lisa Yang Center for Conservation Bioacoustics, Cornell Lab of Ornithology, Cornell University, Ithaca, New York 14850, USA
[2]School of Oceanography, University of Washington, Seattle, Washington 98195, USA
[3]Centre for Geophysical Forecasting, Norwegian University of Science and Technology (NTNU) Gløshaugen, Trondheim, Norway
[4]Université Côte d'Azur, CNRS, Observatoire de la Côte d'Azur, IRD, Géoazur, Sophia Antipolis, 06560, Valbonne, France
[5]FOSINA, Nanterre, France

lea.bouffaut@cornell.edu, qgoestch@uw.edu, robin.a.rorstadbotnen@ntnu.no, sladen@geoazur.unice.fr, arthur.hartog@fosina.fr, Holger.Klinck@cornell.edu

Abstract: Distributed acoustic sensing (DAS) is a promising technology for underwater acoustics, but its instrumental response is still being investigated to enable quantitative measurements. We use fin whale 20 Hz calls to estimate the conversion between DAS-recorded strain and acoustic pressure. Our method is tested across three deployments on varied seafloor telecommunication cables and ocean basins. Results show that after accounting for well-established DAS response factors, a unique value for water compressibility provides a good estimate for the conversion. This work represents a significant step forward in characterizing DAS for marine monitoring and highlights potential limitations related to instrument noise floor.

[Editor: David R. Barclay] https://doi.org/10.1121/10.0036351

Received: 20 December 2024 **Accepted:** 14 March 2025 **Published Online:** 9 April 2025

1. Introduction

Distributed acoustic sensing (DAS) re-purposes existing fiber optic cables into large receiver arrays capable of detecting and localizing underwater acoustic sources, e.g., controlled sources (Douglass *et al.*, 2023; Matsumoto *et al.*, 2021; Shen *et al.*, 2024), ships (Landrø *et al.*, 2022; Rivet *et al.*, 2021), and whales (Bouffaut *et al.*, 2022; Rørstadbotnen *et al.*, 2023; Wilcock *et al.*, 2023). It offers an opportunity for real-time acoustic monitoring over tens of kilometers with a spatial resolution of a few meters. This fiber-sensing technology leverages Rayleigh backscattering and phase shifts in laser pulses to measure distributed strain (see Hartog, 2017, for a comprehensive review). However, the array response is still an open research question.

Lior *et al.* (2021) assessed the capabilities of marine DAS for seismology by comparing ambient sound power spectrum densities up to 30 Hz from data collected by three fiber optic cables to those from existing on-land and underwater broadband seismometers at various locations and depths along each cable. Further research from Matsumoto *et al.* (2021) and Taweesintananon *et al.* (2021) used geo-referenced airgun sources to evaluate DAS frequency response in strain (dimensionless) compared to a hydrophone and seismic streamers. Using a co-located hydrophone, Douglass *et al.* (2023) compared signal-to-noise ratios (SNRs) of signals produced by a broadband bubble pulser. While the literature generally agrees that a DAS strain response for a specific cable-interrogator configuration is influenced by gauge length, signal frequency, wave velocity, and source–receiver grazing angle, the conversion of DAS *RL*s from strain to acoustic pressure remains unsolved. This conversion marks a significant advance in establishing DAS as a quantitative acoustic recorder, building on decades of passive acoustic monitoring research.

This study aims to refine our understanding of the sensitivity and frequency response of DAS to waterborne acoustic signals in the frequency range of low-frequency baleen whale vocalizations. Specifically, we use fin whale 20 Hz calls as reference sources to explore the link between recorded strain and expected acoustic pressure levels. The analysis relies on DAS data collected with different acquisition setups, and located along three different ocean basins: the Northeastern Pacific Ocean, Mediterranean Sea, and North Atlantic Ocean.

[a]Author to whom correspondence should be addressed.

2. Expression of the DAS amplitude response to water-born acoustic signals

DAS uses repeated laser pulses to probe an optical fiber for changes in local strain related to acoustic pressure through the elasticity of the propagation medium. A complete DAS sensing system is composed of (1) an interrogator, the optoelectronic transducer that emits laser pulses (typically, 1550 nm) then converts the returned interferometric light into a digital signal and processes it into strain; (2) an optical fiber that transmits the laser pulse and backscattered light from and to the interrogator; (3) laser-backscattering fiber anomalies, present all along the fiber and reflecting the laser toward the interrogator (Hartog, 2017). Incident pressure waves displace the laser-backscattering anomalies, introducing changes in the optical path length (extracted as a phase shift). The interrogator averages time-differentiated phase change over short fiber sections, namely the gauge length, at regularly spaced intervals along the fiber to create virtual distributed sensing channels. Finally, phase shifts are converted into longitudinal strain waveforms for each corresponding fiber section. The resulting DAS-recorded strain data, sampled in both time and space, is accessible in near-real-time. Current commercial DAS interrogators can typically record nanostrains.

To describe the received level on each DAS channel, we use the formalism of the sonar equation. The received strain level on the DAS array in dB re 1 $\mu\varepsilon$, is expressed as

$$RL_{\mathrm{dB\,re\,1}\,\mu\varepsilon} = RL_{\mathrm{dB\ re\,1}\,\mu\mathrm{Pa}} + S_{\mathrm{Pa}\to\varepsilon} + H_{\mathrm{DAS}_\varepsilon}, \tag{1}$$

where $RL_{\mathrm{dB\,re\,1}\,\mu\mathrm{Pa}}$ is the received pressure level in dB re 1 μPa, $S_{\mathrm{Pa}\to\varepsilon}$ denotes the conversion term in dB between acoustic pressure and the strain measured by DAS, and $H_{\mathrm{DAS}_\varepsilon}$ denotes the response of DAS in dB relative to strain in the bandwidth of the signal of interest, under linear assumptions, assuming a uniform response along the fiber and negligible crosstalk between channels. The received pressure level can be expressed as the combined contributions of the source level of the signal of interest, denoted SL (dB re 1 μPa @1 m) and the transmission loss, TL, which represents the propagation of the acoustic wave between the source and each receiver,

$$RL_{\mathrm{dB\ re\,1}\mu\mathrm{Pa}} = SL + TL. \tag{2}$$

In this work, TL is estimated from the coherent arrivals of the direct and surface-reflected paths (see supplementary material Sec. 1). Finally, the DAS response in strain can be described as the combination of two effects

$$H_{\mathrm{DAS}_\varepsilon} = G_\kappa + G_{\mathrm{GL}}, \tag{3}$$

with G_κ being the coupling between the cable coating and the sensing fiber, and G_{GL} being the effect of the gauge length (GL) (Taweesintananon *et al.*, 2021). The dependency of each term related to, e.g., the grazing angle and gauge length is given in supplementary material Sec. 1. The strain received level described by Eq. (1) takes different values along the whole DAS array. Combining the received pressure level [Eq. (2)] and DAS response [Eq. (3)] equations into Eq. (1) gives a complete overview of the effects considered in our analysis of DAS *RL*s in dB strain,

$$RL_{\mathrm{dB\,re\,1}\,\mu\varepsilon} = SL + TL + S_{\mathrm{Pa}\to\varepsilon} + G_\kappa + G_{\mathrm{GL}}. \tag{4}$$

Conversely, the conversion of DAS-recorded data into pascals (Pa) is

$$RL_{\mathrm{DAS\ dB\ re\ 1}\,\mu\mathrm{Pa}} = RL_{\mathrm{dB\,re\,1}\,\mu\varepsilon} - H_{\mathrm{DAS}_\varepsilon} + S_{\varepsilon\to\mathrm{Pa}}, \tag{5}$$

where $S_{\varepsilon\to\mathrm{Pa}} = -S_{\mathrm{Pa}\to\varepsilon}$ is the conversion factor from strain to Pa in dB. Based on the expression of each independent term given in supplementary material Sec. 1, the total DAS response to an incident wave with a given frequency and sound speed is a function of the elasticity of the medium, the grazing angle, coupling, and gauge length. The frequency range of validity for this proposed framework is discussed in Sec. 6.

3. Description of the datasets

The data used in this work were collected at three locations (Fig. 1) across the North Pacific Ocean (Ocean Observatories Initiative, OOI South) (Wilcock *et al.*, 2023), North Atlantic Ocean (Svalbard) (Rørstadbotnen *et al.*, 2023), and Mediterranean Sea (MedSea) (Rivet *et al.*, 2021), with respective recording parameters summarized in see supplementary material Sec. 2 (Bouffaut *et al.*, 2025). Each independent dataset provided access to a unique DAS configuration with variability in depth range, seafloor sediments, length of the instrumented fiber, and gauge length. Cable armor was unknown but expected to vary with depth (Carter *et al.*, 2009). Channel spacing and sampling frequencies were harmonized in a pre-processing stage (Sec. 4).

These datasets contained recordings of fin whale 20 Hz calls, a regularly produced <1 s downsweep, with frequencies around 20 Hz, believed to be produced exclusively by males. Fin whale 20 Hz calls have been reported with an average SL of $\simeq$189 dB re 1 μPa @1 m (see review in supplementary material Sec. 3). Variations are observed in call center frequencies and inter-call intervals between distinct acoustic populations, e.g., in the North Atlantic (Romagosa *et al.*, 2024), MedSea (Best *et al.*, 2022), and North East Pacific (Oleson *et al.*, 2014). Fin whales have been reported to produce these vocalizations at a depth of 15–20 m (Stimpert *et al.*, 2015). Fin whale 20 Hz calls were used as a well-characterized source of opportunity in this work. Data were first scanned visually during a day with known fin whale presence (from

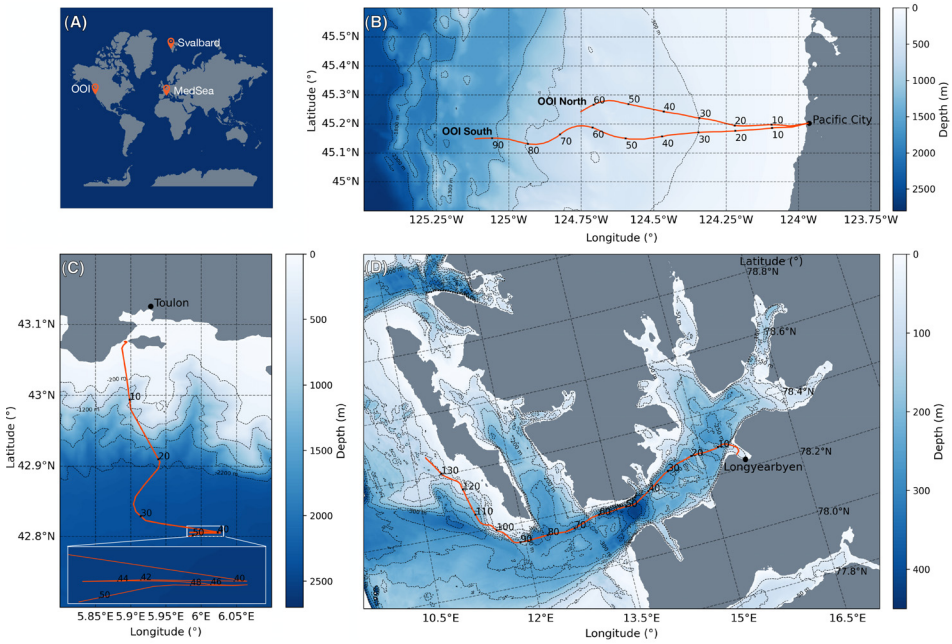

Fig. 1. (A) Overview and (B)–(D) bathymetric maps of the arrays used to test the conversion of DAS-recorded strain into pascals. DAS arrays are spread across three locations. (B) OOI North and South DAS out of Pacific City, Oregon, USA in the North East Pacific Ocean, $GL = 51$ m, (C) MedSea DAS out of Toulon, France, in the Mediterranean Sea, $GL = 4$ m, (D) Svalbard DAS out of Longyearbyen, on Spitsbergen, Norway in the North Atlantic Ocean, $GL = 8$ m. Bathymetric data from GEBCO Compilation Group (GEBCO, 2024).

previous analysis) to select a vocalization from each configuration, aiming for a variety of offsets, a high signal-to-noise ratio where a call is received and visible on multiple DAS channels, and no overlapping vocalizations from other whales. The selected OOI South fin whale 20 Hz data were recorded on November 2, 2021 at 19:00 UTC, MedSea data were recorded on September 22, 2023 at 09:13 UTC, and Svalbard data were recorded on August 22, 2022 at 12:39 UTC.

4. Extracting the amplitude level of fin whale 20 Hz calls along DAS arrays

4.1 Data processing workflow

To investigate the amplitude response of the DAS sensors, the data underwent multiple steps to account for instrument-specific variations in output, isolate fin whale 20 Hz calls, and correct for the source–receiver geometry. These different steps are highlighted in Fig. 2 and detailed in the remainder of this section. Data were pre-processed using the DAS4Whales Python package (Bouffaut, 2023) to harmonize temporal and spatial sampling. Each file was conditioned by (1) loading and converting data to strain (interrogator-dependent), (2) resampling data in time ($f_s = 200$ Hz) and space (channel spacing = 8 m) and, (3) applying a combined frequency-wave number (f–k) (1450–3300 m/s, designed with taper providing gradual attenuation ±150 m/s from the selected speeds to minimize artifacts) and bandpass filter (14–30 Hz) to isolate fin whale 20 Hz calls propagating in the water and sediments.

Pre-processed data were then labeled using a custom tool to match theoretical arrival times with recorded data in the spatiotemporal domain (see supplementary material Sec. 4). The theoretical arrival times were calculated accounting

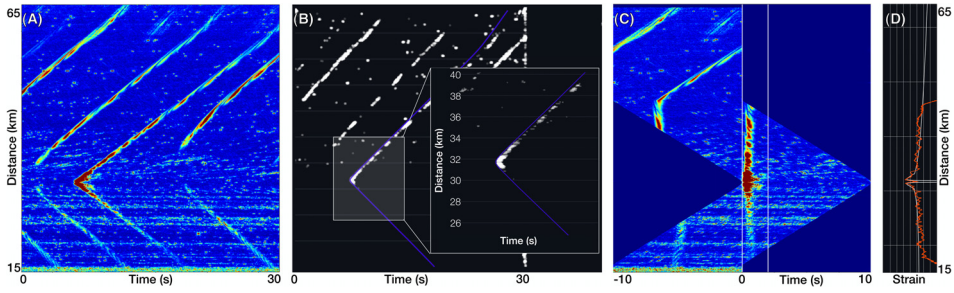

Fig. 2. Schematics of the data analysis pipeline where (A) raw data are pre-processed, (B) manually labeled, (C) time-compensated, to produce (D) a measurement of the DAS response in strain to a fin whale 20 Hz call. The is illustrated on OOI North data, on 2021-11-02 at 17 28 15 UTC.

for depth variations, the three-dimensional (3D) distance between the whale and each DAS channel, and assuming a constant sound speed of $c = 1490$ m/s for all configurations. The annotator defined the apex (channel of the first time of arrival), offset (distance between the whale and the DAS at the apex), and first time of arrival based on the match between the curves. When the cable geometry was sufficiently asymmetric, the annotator could determine the side of the source relative to the cable.

The pre-processed data were time-aligned in the final processing step, compensating for theoretical travel times associated with the labels. This step aimed to isolate the first arrival pair (direct and surface-reflected paths), limiting the analysis to a single set of grazing angles. We used the call-associated labels to retrieve theoretical arrival times. The compensation was performed on a 10 s window, chosen to enable the analysis of a received signal over $\simeq$15 km on each side of the apex [Fig. 2(C)]. Each call-associated DAS strain received level was then estimated by averaging the amplitude over a 2 s window, ensuring the capture of the entire signal (<1 s) and accommodating for some potential offset or c error. The noise level (NL) was also estimated on a 2 s window within the minute preceding the call, applying an identical time compensation and ensuring no overlap with other calls. Code supporting this work is available in open access (Bouffaut, 2025).

4.2 Fixed parameters and approximations used in our calculation of the amplitude response of DAS

Our simulations of DAS RLs used several fixed variables and approximations that are further discussed in Sec. 6.1. The transition range (r_T), the distance at which sound propagation transitions from spherical to cylindrical (Duncan and Parsons, 2011), was empirically set to $n\times$ water depth at the apex with $n = 4$ for OOI South and MedSea, and $n = 8$ in Svalbard. Fin whale 20 Hz calls were considered to be produced with a central frequency of 20 Hz at a depth $z_{\text{whale}} = 20$ m (Stimpert *et al.*, 2015) with a source level $SL = 189$ dB re 1 μPa @ 1 m (see supplementary material Sec. 4). The sound speed in the water was fixed at a standard $c = 1490$ m/s. For DAS data, we followed the approach by Taweesintananon *et al.* (2021) by considering the pulse width equal to the gauge length of each configuration (supplementary material Sec. 2), and setting the ratio between the Young's modulus of the cable and fiber $\alpha = 0.8$ as the cable is expected to have a smaller effective Young's modulus than the fiber (supplementary material Sec. 1). Supplementary material Sec. 6 presents a sensitivity analysis on the effect of c, z_{whale} and α on DAS response.

5. Results: Comparison of the recorded and simulated DAS amplitude responses

We analyzed fin whale 20 Hz calls recorded at three locations: the call recorded on the OOI South data was estimated with an apex of 31.95 km and an offset of 340 m, the one on MedSea with an apex of 35.35 km and an offset of 2375 m, and the one from Svalbard with an apex of 79.0 km and an offset of 1500 m. Figure 3 illustrates the different contributions

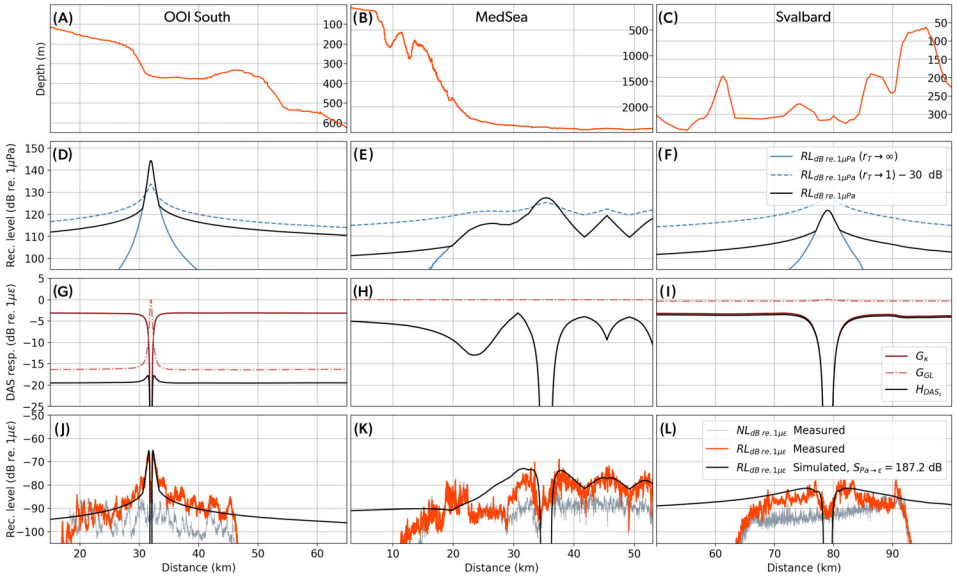

Fig. 3. Fin whale 20 Hz calls received along three DAS arrays in the North East Pacific Ocean [OOI South; (A), (D), (G), (J) apex: 32 km, offset: 0.3 km], the Mediterranean Sea [MedSea (B), (E), (H), (K); apex: 35 km, offset: 2.4 km], and the North Atlantic Ocean [Svalbard (C), (F), (I), (L); apex: 79 km, offset of 1.5 km]. (A)-(C) Bathymetry along each array. RLs on DAS result from the combination of (D)-(F) the pressure levels received on the cable $RL_{\text{dB re 1 }\mu\text{Pa}}$, simulated following Eq. (2), (G)-(I) the instrument response $H_{\text{DAS}_\varepsilon}$ in dB re 1 $\mu\varepsilon$, simulated following Eq. (3), and, a conversion factor between pressure and strain $S_{\text{Pa}\to\varepsilon}$, (J)-(L) comparison between measured and simulated RLs on DAS in dB re 1 $\mu\varepsilon$, overlaid with measured NLs. DAS RLs are simulated following Eq. (4) with a unique conversion factor $S_{\text{Pa}\to\varepsilon} = 187.2$ dB.

to DAS *RL*s expressed in Eq. (1) for these three DAS arrays. On OOI South and MedSea, the offset of the whale and local depth at the location of the apex [Figs. 3(A) and 3(B)] were equivalent, which corresponds to the nearest possible offset resolution. For Svalbard, the whale vocalized at an offset close to five times the local bathymetry.

Figures 3(D)–3(F) represent the received pressure levels along the fiber. They illustrate the effects of spherical spreading combined with the interference field ($r_T \to \infty$) and cylindrical spreading ($r_T \to 1$). Note that a 30 dB offset was subtracted from $RL_{\mathrm{dB\,re\,1\,\mu Pa}}$ ($r_T \to 1$) only for graphical purposes. The resulting $RL_{\mathrm{dB\,re\,1\,\mu Pa}}$ for OOI South shows a rapid amplitude decrease in the vicinity of the apex, with a slightly asymmetrical transition range between the left and right side due to positive depth gradient close to the apex [Fig. 3(A)]. For MedSea, most of the analyzed DAS section is in the spherical propagation range (except under 20 km), where the abrupt variations are related to the "W" shape of the DAS array between 40–52 km. For Svalbard, the increased whale offset introduces a more gentle slope to the spherical amplitude decay.

Figures 3(G)–3(I) illustrate the effects of the coupling, G_ε, and gauge length, G_{GL}, that are both dependent on the grazing angle θ (supplementary material Sec. 1). The sum of these two terms, $H_{\mathrm{DAS}_\varepsilon}$, represents the DAS response. For all sites, $G_\varepsilon \to -\infty$ in the vicinity of the apex. G_{GL} is only significant for OOI South where the gauge length is much larger than at the other sites (51 m against 4 and 8 m), causing $\simeq$16 dB attenuation just a few kilometers away from the apex, when θ becomes small. With the additional G_ε term, the amplitude response at OOI South is reduced by nearly 20 dB at all distances, with no sensitivity to direct waves at the apex. At the other two sites, G_{GL} is close to zero because of the small gauge lengths relative to the wavelength of the signal. $H_{\mathrm{DAS}_\varepsilon}$ is then dominated by G_ε that demonstrates a strong sensitivity to changes in θ. The width of the sensitivity gap at the apex is also dependent on θ, which increases with offset at a set configuration.

Finally, Figs. 3(J)–3(L) compare simulated [following Eq. (4)] and measured received strain levels. Overall, we were able to reproduce the main trends in the amplitude response of the DAS measurements using a unique conversion factor $S_{\mathrm{Pa}\to\varepsilon} = 187.2$ dB. In particular, there is good agreement near the apex, where combined effects strongly impact the measured signal. Away from the apex, the propagation loss trends match the observed signal decays but do not capture smaller local amplitude variations. Note the drop in amplitude, e.g., close to 19 and 46 km on OOI South, is related to our choice of analysis window (10 s) that reduces the range of valid distances to less than $\pm$15 km around the apex [see Figs. 2(C) and 2(D)]. The comparison to the measured noise *NL* was used to interpret potential trends in $RL_{\mathrm{dB\,re\,1\,\mu\varepsilon}}$. For OOI South, the fin whale *RL* blends in noise below $\simeq$22 km while it is received up to the furthest measurement points 14 km away from the apex in deeper waters. MedSea fin whale *RL* is affected by the array geometry: at the furthest distances, there is a good agreement between the simulated and measured levels. However, *RL*s are close to 10 dB under simulated levels between 23 and 29 km and both noise and *RL*s are above the predicted values around 20 km. This DAS setup also presents locations with reduced sensitivities e.g., around 43 and 49 km. Finally, there is a good agreement in predicted and simulated *RL*s in Svalbard with an increased *RL* at 91 km because of the vocalization of another individual. The spatially average noise level was estimated at $-$94 dB between 20 and 45 km on OOI South, $-$90 dB between 23 and 50 km for MedSea, and $-$91 dB between 68 and 90 km in Svalbard. Following Eq. (5), the time-compensated data presented in Figs. 3(J)–(L) can be converted into Pa to match 3(D)-3(F) (supplementary material Sec. 5).

6. Discussion

This study investigates the conversion of DAS-recorded strain to acoustic pressure through the compensation of the DAS response using a unique conversion factor, tested on fin whale 20 Hz calls in heterogeneous recordings from three locations.

6.1 Approximations in the methodology and limitations

The analysis pipeline (Sec. 4) relies on an analyst's estimate of the position of the whale relative to the DAS array (whale apex, offset, and start time) based on time of arrivals and considering a constant sound speed. This method lacks offset resolution for distances smaller than the local bathymetry. It can be imprecise at large offsets, particularly when arrival time fits are defined at channels farther from the apex where assuming a constant sound speed may introduce errors. Some of this potential error is absorbed by the final 2 s average window that enables signals propagating $c = 1490 \pm 60$ m/s to arrive 15 km away from the apex within 0.8 s from each other. Yet, it was chosen for its simplicity and replicability to other DAS deployments on single, straight fibers over more complex localization schemes using two fibers as in Rørstadbotnen *et al.* (2023). Surface-generated coherent interference patterns (Lloyd's mirror effect) could help resolve whale offset and vocalizing depth simultaneously (Pereira *et al.*, 2020) on single fibers. Another localization limitation is the lack of precision in cable positions as they are often based on the trajectory of the cable-laying vessel, which can be improved using a controlled source (Shen *et al.*, 2024).

As a first assumption, whale vocalizing depth was set to a fixed value, similarly to whale source levels and other variables (Sec. 4.2). These values were set at documented reasonable averages to limit the number of parameters in our analysis. Yet, we acknowledge that they may present variability, e.g., fin whale source levels are reported with a standard deviation of 4–6 dB (see supplementary material Sec. 4) and source depth have been shown between 15–20 m on tag data

(Stimpert *et al.*, 2015) and indirectly measured around 70 m (Pereira *et al.*, 2020). Supplementary material Sec. 6 presents a sensitivity analysis of the effects of c, z_{whale} and α on DAS response. The resulting variance is smaller than SL standard deviation, indicating that SL is the dominant source of variability in this study.

We determined the transition range, r_T, along each DAS empirically, which led to four times the water depth in both OOI South and MedSea datasets, but to eight times the water depth in Svalbard. In shallow water, it depends on seabed properties, especially its critical grazing angle (if $\theta < \theta_c$ close to perfect reflection). Softer and less reflective seabeds have smaller critical angles leading to larger values of r_T, matching Svalbard's sedimentology (mostly sludge) compared to the other locations (Duncan and Parsons, 2011).

6.2 Result interpretation and implications

This work considered and modeled direct and surface-reflected coherent propagation paths impinging DAS at the grazing angle θ. *In situ*, 3D propagation of a signal results in multiple sets of arrivals on DAS, originating from bottom-surface, local bathymetry, and sub-seafloor reflections (Bouffaut *et al.*, 2022). This creates a range of grazing angles for a single emission. These additional paths may counteract energy loss for wavefronts normal to the fiber. However, they can also generate additional coherent interferences. Multipath propagation and modal acoustics fields may be responsible for some of the local energy variations observed in Figs. 3(J)–3(L) at all sites (Shen *et al.*, 2024). In the MedSea, the increase in RL (and NL) observed around 20 km, is present on many files; some with distinct times of arrivals, others as a diffused 20 Hz far-field energy band resembling sound fixing and ranging propagation. It is followed by a section of cable where $RL = NL$ $\simeq$29 km. These energy variations could be the effect of the steep bathymetric gradient (these channels are close to 2000 m depth), where acoustic modes excited by the 20 Hz call in deeper water reach a cut-off frequency and therefore dissipate when propagating toward shallower water. There could be some uncertainties on the cable location but the abrupt change at 29 km seems to match with changes in sediments from mud to sandy mud. In comparison to the two other DAS, MedSea also presents several channels, or groups of channels, with reduced sensitivities. For this call, the whale was localized with an apex at 35 km, and a $\simeq$ 2 km offset on the outer end of the fiber (outside of the curve between 20–40 km). Therefore, the observed sensitivity drops at 43 and 49 km are related to small θ on the fiber.

We find that the value $S_{\text{Pa}\to\varepsilon} = 187.2$ dB yields a good agreement between simulated and measured received strain levels. Carter *et al.* (2009) underlines that fiber optic cable protection varies with depth. Nearshore, cables are generally armored and often buried into the seabed (down to $\simeq$1500 m depths) as a protective measure against local hazards, e.g., bottom trawl fishing and shipping activities. The MedSea cable extends below usual burial depths and may also be covered by depositing sediments. There is a frequency range for which the burial depth is transparent to the acoustics wave, i.e., the wavelengths are long enough to ignore the presence of the sediments overlaying the cable so the wavelength received on DAS propagates mostly in water. Assuming a 2m average burial depth and a minimum wavelength of 4$\times$ burial depth to be conservative, the range of validity of the proposed analysis spans $\simeq$0–185 Hz for $c = 1490$ m/s. Using a unique conversion factor $S_{\text{Pa}\to\varepsilon}$, our results show minimal differences in expected and measured $RL_{\text{dB re 1}\,\mu\varepsilon}$ across sites, potential burial depths and sediment types, suggesting a minimal influence of the seabed on DAS response at these frequencies.

Budiansky *et al.* (1979) demonstrated that sensitivity of a bare fiber to pressure is increased by over a tenfold when using cladding as it increases the compressibility of the fiber. Under external pressure, the coated fiber will contract with the coating in the axial direction so that the strain in that direction is mainly controlled by the cladding material, which was tested on a fiber coated with a unique layer of Teflon-like plastic. Yet, modern telecommunication fibers are covered with a succession of materials (see Fig. 2.4 in Carter *et al.*, 2009 for cross sections note that the diameter of double-armored cables < 50 mm is currently the maximum level of protection and uses galvanized steel). A thorough assessment of the impact of cladding and protective layers on the sensitivity of the fiber requires analytical or modeling solutions, particularly for some cable structures, e.g., loose fiber in a steel tube. Without gel, the pressure might not be transmitted to the fiber and the dominant effect of an incoming pressure wave would be through elongation of the cable. In our analysis, we integrated the relationship between the fiber and coating materials in the coupling term, G_K, with grazing angle dependency and incorporating a ratio of the Young's moduli of the cable and fiber, which provides a reasonable approximation of the response at all sites. Note that detailed information on the composition of fiber optic cables used for DAS is scarcely available.

We suggest that the conversion from dimensionless strain, ε, to pressures, p, in Pa could depend on the water compressibility for water-propagated acoustic signals $<$185 Hz. Water compressibility is expressed by the bulk modulus K_{water}, such as $\varepsilon = p/K_{\text{water}}$, at each array element varying as a function of temperature and depth (Safarov *et al.*, 2009). A $K_{\text{water}} \in 2.2 - 2.5 \times 10^9$ Pa provides close values when converted to dB, $S_{\varepsilon\to\text{Pa}} = 20\log_{10}K_{\text{water}} \in 186.8 - 188.0$ dB.

We noted that in contrast to shorter gauge lengths, the larger gauge length of OOI South lowers the DAS response [Fig. 3(G)]. A 51 m gauge length is not negligible compared to the $\simeq$75 m wavelength of the signal. This observation is in agreement with the frequency-dependent impact of the gauge length described by Dean *et al.* (2017) at $\theta = 0$, where G_{GL} decreases to a first $G_{\text{GL}} \to -\infty$ notch at multiples of $c/GL \simeq 29$ Hz. However, long gauge lengths (in comparison to the wavelength of the signal) enable a better averaging of incoherent optical noise improving the SNRs of coherent

acoustic waves even in under-optimal settings, especially when the apparent wavelength increases away from the apex (Dean *et al.*, 2017). This trend of lower noise levels for longer gauge lengths is verified by our measurements, where the *NL* obtained on data from OOI South is 3–4 dB lower than on the other DAS. Yet, this reduction may also be due to other factors, such as ocean noise variability (Shen *et al.*, 2024) or various instrumental noise floors. From Figs. 3(J)–3(L), the difference between maximum *RL* and averaged *NL* is 30 dB for OOI, 15 dB for MedSea, and about 10 dB in Svalbard. These differences reported to our simulated received pressure levels gives an average noise measurement between ≃95–112 dB re 1 μPa across sites, which is above expected noise levels at these frequencies. The *NL* increase along the fiber is also observed in other Svalbard publications (e.g., Landrø *et al.*, 2022; Taweesintananon *et al.*, 2023) and could be the result of long-range DAS implementation. These first estimates of instrument noise floors raise a potential limit in the detection range of water-borne acoustic signals, the maximum source–receiver distance for a signal to be detected, as they seem to be 20–30 dB higher than the expected ambient noise levels.

Supplementary Material

See the supplementary material for (1) an overview of theory behind DAS sonar equation, (2) data collection parameters for each DAS, (3) a review of fin whale source levels, (4) a description of our custom annotation tool, (5) an illustration of DAS data converted into Pa, and (6) a sensitivity analysis of the parameters of our model.

Author Declarations

Conflict of Interest

The authors have no conflicts to disclose.

Data Availability

The data and code that support the findings of this study are openly available (Bouffaut, 2025; Bouffaut *et al.*, 2025).

References

Best, P., Marxer, R., Paris, S., and Glotin, H. (**2022**). "Temporal evolution of the Mediterranean fin whale song," Sci. Rep. **12**(1), 13565.

Bouffaut, L. (**2023**). "Das4whales: A Python package to analyze distributed acoustic sensing (DAS) data for marine bioacoustics (v0.1.0)." Zenodo. https://doi.org/10.5281/zenodo.7760187.

Bouffaut, L. (**2025**). "Das4whales/das_levels: First release," Zenodo. https://doi.org/10.5281/zenodo.15008957.

Bouffaut, L., Goestchel, Q., Sladen, A., Hartog, A., and Klinck, H. (**2025**). "Distributed acoustic sensing fin whale labeled dataset level estimations." Zenodo. https://doi.org/10.5281/zenodo.15008561.

Bouffaut, L., Taweesintananon, K., Kriesell, H. J., Rørstadbotnen, R. A., Potter, J. R., Landrø, M., Johansen, S. E., Brenne, J. K., Haukanes, A., Schjelderup, O., and Storvik, F. (**2022**). "Eavesdropping at the speed of light: Distributed acoustic sensing of baleen whales in the arctic," Front. Mar. Sci. **9**, 901348.

Budiansky, B., Drucker, D., Kino, G., and Rice, J. (**1979**). "Pressure sensitivity of a clad optical fiber," Appl. Opt. **18**(24), 4085–4088.

Carter, L., Burnett, D., Drew, S., Marle, G., Hagadorn, L., Bartlett-McNeil, D., and Irvine, N. (**2009**). "Submarine cables and the oceans–Connecting the world," in *UNEP-WCMC Biodiversity Series* (ICPC/UNEP/UNEP-WCMC), pp. 17–25.

Dean, T., Cuny, T., and Hartog, A. H. (**2017**). "The effect of gauge length on axially incident p-waves measured using fibre optic distributed vibration sensing," Geophys. Prospect. **65**(1), 184–193.

Douglass, A. S., Abadi, S., and Lipovsky, B. P. (**2023**). "Distributed acoustic sensing for detecting near surface hydroacoustic signals," JASA Express Lett. **3**(6), 066005.

Duncan, A., and Parsons, M. (**2011**). "How wrong can you be? Can a simple spreading formula be used to predict worst-case underwater sound levels?," in *Proceedings of the Annual Conference of the Australian Acoustical Society,* 2–4 November 2011, Gold Coast, Australia, pp. 1–8., pp. 1–8.

GEBCO Compilation Group (**2024**). "GEBCO 2024 grid," doi: https://doi.org/10.5285/1c44ce99-0a0d-5f4f-e063-7086abc0ea0f, Dataset (2024).

Hartog, A. H. (**2017**). *An Introduction to Distributed Optical Fibre Sensors*, 1st ed. (CRC Press, Boca Raton, FL).

Landrø, M., Bouffaut, L., Kriesell, H. J., Potter, J. R., Rørstadbotnen, R. A., Taweesintananon, K., Johansen, S. E., Brenne, J. K., Haukanes, A., Schjelderup, O., and Storvik, F. (**2022**). "Sensing whales, storms, ships and earthquakes using an arctic fibre optic cable," Sci. Rep. **12**(1), 19226.

Lior, I., Sladen, A., Rivet, D., Ampuero, J., Hello, Y., Becerril, C., Martins, H. F., Lamare, P., Jestin, C., Tsagkli, S., and Markou, C. (**2021**). "On the detection capabilities of underwater distributed acoustic sensing," JGR Solid Earth **126**(3), e2020JB020925.

Matsumoto, H., Araki, E., Kimura, T., Fujie, G., Shiraishi, K., Tonegawa, T., Obana, K., Arai, R., Kaiho, Y., Nakamura, Y., Yokobiki, T., Kodaira, S., Takahashi, N., Ellwood, R., Yartsev, V., and Karrenbach, M. (**2021**). "Detection of hydroacoustic signals on a fiber-optic submarine cable," Sci. Rep. **11**(1), 2797.

Oleson, E. M., Širović, A., Bayless, A. R., and Hildebrand, J. A. (**2014**). "Synchronous seasonal change in fin whale song in the North Pacific," PLoS One **9**(12), e115678.

Pereira, A., Harris, D., Tyack, P., and Matias, L. (**2020**). "On the use of the Lloyd's Mirror effect to infer the depth of vocalizing fin whales," J. Acoust. Soc. Am. **148**(5), 3086–3101.

Rivet, D., de Cacqueray, B., Sladen, A., Roques, A., and Calbris, G. (**2021**). "Preliminary assessment of ship detection and trajectory evaluation using distributed acoustic sensing on an optical fiber telecom cable," J. Acoust. Soc. Am. **149**(4), 2615–2627.

Romagosa, M., Nieukirk, S., Cascão, I., Marques, T. A., Dziak, R., Royer, J.-Y., O'Brien, J., Mellinger, D. K., Pereira, A., Ugalde, A., Papale, E., Aniceto, S., Buscaino, G., Rasmussen, M., Matias, L., Prieto, R., and Silva, M. A. (**2024**). "Fin whale song evolution in the North Atlantic," eLife **13**, e83750.

Rørstadbotnen, R. A., Eidsvik, J., Bouffaut, L., Landrø, M., Potter, J., Taweesintananon, K., Johansen, S., Storevik, F., Jacobsen, J., Schjelderup, O., Wienecke, S., Johansen, T. A., Ruud, B. O., Wuestefeld, A., and Oye, V. (**2023**). "Simultaneous tracking of multiple whales using two fiber-optic cables in the Arctic," Front. Mar. Sci. **10**, 1130898.

Safarov, J., Millero, F., Feistel, R., Heintz, A., and Hassel, E. (**2009**). "Thermodynamic properties of standard seawater," Ocean Sci. **5**(3), 235–246.

Shen, Z., Wu, W., and Lin, Y.-T. (**2024**). "High-resolution observations of shallow-water acoustic propagation with distributed acoustic sensing," J. Acoust. Soc. Am. **156**(4), 2237–2249.

Stimpert, A. K., DeRuiter, S. L., Falcone, E. A., Joseph, J., Douglas, A. B., Moretti, D. J., Friedlaender, A. S., Calambokidis, J., Gailey, G., Tyack, P. L., and Goldbogen, J. A. (**2015**). "Sound production and associated behavior of tagged fin whales (*Balaenoptera physalus*) in the Southern California Bight," Anim. Biotelemetry **3**(1), 23.

Taweesintananon, K., Landrø, M., Brenne, J. K., and Haukanes, A. (**2021**). "Distributed acoustic sensing for near-surface imaging using submarine telecommunication cable: A case study in the Trondheimsfjord, Norway," Geophysics **86**(5), B303–B320.

Taweesintananon, K., Landrø, M., Potter, J. R., Johansen, S. E., Rørstadbotnen, R. A., Bouffaut, L., Kriesell, H. J., Brenne, J. K., Haukanes, A., Schjelderup, O., and Storvik, F. (**2023**). "Distributed acoustic sensing of ocean-bottom seismo-acoustics and distant storms: A case study from Svalbard, Norway," Geophysics **88**(3), B135–B150.

Wilcock, W. S., Abadi, S., and Lipovsky, B. P. (**2023**). "Distributed acoustic sensing recordings of low-frequency whale calls and ship noise offshore central oregon," JASA Express Lett. **3**(2), 026002.